PNAS
www.pnas.org

Supplementary Information for

C. elegans DSB-3 Reveals Conservation and Divergence among Protein Complexes Promoting Meiotic Double-Strand Breaks

Albert W. Hinman[1,2], Hsin-Yi Yeh[3], Baptiste Roelens[1], Kei Yamaya[1], Alexander Woglar[1], Henri-Marc G. Bourbon[4], Peter Chi[3,5], Anne M. Villeneuve[1,2,*]

*Correspondence: annev@stanford.edu

This PDF file includes:

Supplementary Information Text

Supplementary Materials and Methods

C. elegans strains
Strains were cultured at 20℃ using standard nematode growth conditions (1) unless otherwise noted. Strains used in this study:

AV28 *dsb-3(me6ts)* IV
AV776 *spo-11(me44) IV / nT1[qIs51]* (IV;V)
AV818 *meIs8[gfp::cosa-1]* II; *cosa-1(tm3298)* III
AV913 *dsb-3(me6ts)* IV
AV958 *dsb-3(me6ts) dpy-20(e1282)* IV
AV994 *dpy-3(e184) dsb-3(me6ts)* IV
AV995 *dsb-3(me115) IV / nT1 (*IV;V)
* AV1029 *meSi7* [*sun1p::dsb-3::gfp::sun-1 3'UTR] II; dsb-3(me115) IV*
AV1045 *meSi7 II; dsb-3(me115) dsb-1(we11) / nT1 IV*
AV1081 *meSi7 dsb-2(me96) / mnC1 II; dsb-3(me115) IV*
AV1095 *dsb-3(me115) / tmC5 [F36H1.3(tmIs1220)]* IV
^ AV1102 *dsb-1(me124[3xha::dsb-1]) dsb-3(me125[3xflag::dsb-3]) IV*
^ AV1115 *dsb-2(me132)[3xha::dsb-2] II*
AV1132 *meIs8[gfp::cosa-1]* II*; cosa-1(tm3298)* III*; dsb-3(me115)* IV */ nT1* (IV;V)
Bristol N2 Wild type

* The transgene allowing expression of the DSB-3::GFP fusion protein was obtained using the Mos Single Copy Insertion strategy (MosSCI, (2)) using the *ttTi5605* insertion on chromosome II as a landing site. The donor plasmid, pBR253, was obtained by assembling fragments carrying the upstream promoter region of the *sun-1* gene, the *sun-1* downstream 3'UTR region, and the genomic sequence of *dsb-3* (coding exons and introns), together with a DNA fragment containing a version of GFP optimized for germline expression (3), into pBR49, a derivative of pCFJ350 modified to enable type IIs restriction/ligation cloning (4). The genomic fragments were obtained by PCR amplification of wild-type genomic DNA using the following primer pairs. The primers for the *sun-1* promoter were oBR840 (cgtcgatgcacaatccGGTCTCaCCTGatttccagatttcatcgtcggtttt) and oBR841 (agtggaatgtcagGGTCTCaCATaccgagtagatctggaagtttag). The primers for *dsb-3* CDS were: oBR836 (cgtcgatgcacaatccGGTCTCaTATGATCGAAATTACCGATGATGAGG) and oBR837 (agtggaatgtcagGGTCTCaCTCCATTGCTATATCTCTGTTGATTATCTAAAAAC) The primers for the *sun-1* 3'UTR were oBR842 (cgtcgatgcacaatccGGTCTCaTAAAaaacgccgtattattgttcctgc) and oBR843 (agtggaatgtcagGGTCTCaGTCAttagtaagttaaagctaaagttagcag). The GFP fragment was obtained by PCR amplification of pCFJ1848 (3), using oBR406 (cgatgcacaatccGGTCTCaGGAGGTGGATCATCCTCCACATCATCCT) and oBR407 (agtggaatgtcagGGTCTCaTTTATGGGGAAGTACCGGATGACG). Correct assembly of all fragments within the donor plasmids was verified by sequencing.

^ In order to perform pairwise colocalization experiments between DSB-1, DSB-2 and DSB-3, we created strains expressing endogenously-tagged versions of these proteins so each pair could be detected using compatible primary antibodies generated in different host organisms. For these strains, we used direct injection of Cas9 protein (PNAbio) complexed with single-guide RNA (sgRNA) (Dharmacon) using the protocol of (5). CRISPR targeting (crRNA) sequences were designed using Benchling (https:// benchling.com/). Small single-stranded oligonucleotides (< 200 bp) were purchased (Integrated DNA Technologies) and used as the repair templates to generate the various tags and nonsense alleles. N2 worms (P0) were injected with the mix together with sgRNA and repair

template for the *dpy-10* co-CRISPR marker (6). Rol F1s (carrying *dpy-10(Rol)* marker) were singled out, and a subset of F2 progeny was fixed and stained with DAPI (see below) to assess the phenotype of diakinesis nuclei for null alleles. From plates containing worms exhibiting univalents at diakinesis, the new mutations were recovered from siblings of the imaged worms and balanced by *nT1* IV or *tmc5* IV. Tagged alleles were confirmed by immunofluorescence staining (see below). All edits were confirmed by Sanger sequencing of PCR fragments amplified using primers designed to detect the edit event. The crRNAs used, description of the edits, and PCR sequencing primers used are included in Supplemental Table 1.

Isolation, mapping, and genomic identification of the *dsb-3(me6ts)* mutation

dsb-3(me6ts) was isolated in a genetic screen for meiotic mutants exhibiting a high incidence of males as described in (7). After backcrossing (four times) to generate the AV913 strain, homozygous *me6ts* worms were subjected to whole-genome sequencing. DNA was extracted from ~8 60mm confluent plates of N2 and AV913 gravid adult worms; worms were rinsed twice in M9 and resuspended in 10 mM EDTA and 0.1 M NaCl. Worms were then: pelleted; flash frozen in liquid nitrogen; resuspended in 450 µL of lysis buffer containing 0.1 M Tris, pH 8.5, 0.1 M NaCl, 50 mM EDTA, and 1% SDS plus 40 µL of 10 mg/mL proteinase K in TE (10 mM Tris, 1 mM EDTA), pH 7.4; vortexed; and incubated at 62°C for 45 min. Two successive phenol-chloroform extractions were performed using the Phase Lock gel tubes from Invitrogen, and DNA was precipitated with 1 mL of 100% ethanol plus 40 µL of saturated NH_4Ac (5 M) and 1 µL of 20 mg/mL GlycoBlue. The DNA pellet was washed with 70% ethanol, air dried, and resuspended in 50 µL of TE, pH 7.4. Paired end libraries were prepared using the Nextera technology (Illumina), and sequencing was performed on an MiSeq sequencer (2 × 75 bp) through the Stanford Functional Genomics Facility. To analyze the genomic data, we used an analysis pipeline adapted from GATK's recommended best practices (8–10). Reads were mapped to *C. elegans* reference genome (WBcel 235.82) using the Bowtie 2 software (11). Variant calling was performed using Haplotype Caller software from GATK, and lists from AV913 and N2 were compared to eliminate non-causal variants. The predicted effects of variants specific to AV913 were then annotated using SnpEff (12).

Initial genetic mapping experiments had placed *dsb-3(me6ts)* within 2 cM of *unc-5*, located at 1.78 cM on chromosome IV; the above sequence analysis identified several candidate mutations within this region. Additional mapping crosses located *dsb-3(me6ts)* to the left of *dpy-20* (at 5.22 cM) and near or to the left of *unc-24* (at 3.51 cM). Further, we found that *eDf18* (which deletes the region between 3.7- 4.19 cM) complements *dsb-3(me6ts)*. Together, these experiments identified a G -> A transition at genomic position IV: 7758710 (WS279), in the second coding exon of the uncharacterized gene *C46A5.5*, as the likely causal mutation responsible for the *dsb-3(me6ts*) mutant phenotype.

DAPI staining of oocyte chromosomes and Irradiation Assay

Numbers of DNA bodies present in diakinesis oocytes were assessed in intact adult hermaphrodites of the indicated ages, raised at the indicated temperatures, fixed in ethanol and stained with 4′,6-diamidino-2-phenylindole (DAPI) as in (13). This method underestimates the frequency of achiasmate chromosomes, as some univalents lie too close to each other to be resolved unambiguously.

To test for rescue of bivalent formation by exogenously derived DSBs, worms were exposed to 5,000 rad (50 Gy) of γ-irradiation using a Cs-137 source at 20 h post-L4 stage. Worms were fixed and stained at 18–20 h post-irradiation, and numbers of DAPI bodies were counted in oocyte nuclei in the -1 to -3 positions.

Bioinformatic identification of homology between DSB-3 and Mei4

PSI Blast searches using the MPI BLAST server (14) , initiated using an alignment of DSB-3 homologs from diverse roundworm species as the query, identified a putative *Brugia malayi* DSB-3 homolog. A subsequent round of PSI-BLAST searches, initiated using an alignment with the putative *B. malayi* homolog as the header sequence and initially focusing on the N-terminal portion of the

protein, led to retrieval of plant and animal Mei4 homologs. Similarity in protein lengths and patterns of predicted secondary structure were prioritized over E-value considerations in selection of proteins chosen for the multiple sequence alignment presented in Supplemental Figure 2, which was generated using MAFFT Version 7.0 with gap opening penalty parameter set to 2.0 and offset value parament set to 0.125.

Yeast Two-Hybrid Analysis

Full-length DSB-1, DSB-2, DSB-3, and N-terminally truncated SPO-11 (SPO-11Δ1-47), DSB-1 (DSB-1Δ1-33) ORFs were individually cloned into the *Bam*HI and *Pst*I sites of pBridge, and the *Bam*HI and *Xho*I sites of pGADT7 (Clontech) to generate fusion proteins with the N-terminal Gal4 DNA-binding domain (Gal4BD) or activation domain (Gal4AD). The PJ69-4A yeast strain (*MATa trp1-901 leu2-3,112 ura3-52 his3-200 gal4Δ gal8Δ GAL2-ADE2 LYS2::GAL1-HIS3 met2::GAL7-lacZ*) was co-transformed with the indicated pairs of constructs encoding Gal4BD and Gal4AD fusion proteins (and/or empty vector negative controls). Transformed cells expressing Gal4BD and Gal4AD fusion proteins were selected in SD-Leu$^-$Trp$^-$, a drop-out medium without leucine and tryptophan. Protein interactions were assayed by growing transformed cells for 5 days at 30°C on selective media lacking leucine, tryptophan, histidine, and adenine (SD-Leu$^-$Trp$^-$His$^-$Ade$^-$). Three independent repeats of each transformation were performed for all pairwise combinations. The full-length SPO-11 ORF was excluded from analysis of combinations as it exhibited autoactivation in negative control experiments.

Immunofluorescence Methods

The following primary antibodies were used: mouse anti-HA (1:1000, Covance 16B12 clone), rabbit anti-FLAG (1:5000, Sigma Aldrich), rabbit anti-DSB-2 (1:5.000, (15)), guinea pig anti-DSB-1 (1:500, (16)), rabbit anti-GFP (1:200, (17)), guinea pig anti-HIM-8 (1:500, (18)), chicken anti-HTP-3 (1:400, (19)), rabbit anti-SYP-2 (1:200, (20)), rat anti-RAD-51 (1:500, (15)), guinea pig anti-SUN-1 S24pi (1:700, (21)), chicken anti-GFP (1:500, (A01694, Genscript)). Secondary antibodies were Alexa Fluor 488, 555 and 647-conjugated goat antibodies directed against the appropriate species (1:400, Life Technologies).

For immunofluorescence experiments involving whole mount gonads, dissection of gonads, fixation, immuno-staining and DAPI counterstaining were performed as in (22) .

For experiments involving nuclear spreads, spreading was performed as in (23). The gonads of 20–100 adult worms were dissected in 10 µL Dissection solution (75% v/v Hank's Balanced Salt Solution [HBSS, Life Technology, 24020-117] with 0.1% v/v Tween-20) on an ethanol-washed plain slide. 50 µL of spreading solution (32 µL of Fixative [4% w/v Paraformaldehyde and 3.2%–3.6% w/v Sucrose in water], 16 µL of Lipsol solution [1% v/v in water], 2 µL of Sarcosyl solution [1% w/v of Sarcosyl in water]) were added, and gonads were immediately distributed over the whole slide using a pipette tip. Slides were then left to dry at room temperature overnight, washed for 20 minutes in methanol at -20°C and rehydrated by washing 3 times for 5 minutes in PBS-T. A 20-minute blocking in 1% w/v BSA in PBS-T at room temperature was followed by overnight incubation with primary antibodies at room temperature (antibodies diluted in: 1% w/v BSA in PBS-T). Slides were washed 3 times for 5 minutes in PBS-T before secondary antibody incubation for 2 hours at room temperature. After PBS-T washes, the samples were mounted in Vectashield (Vector).

To dissect large quantities of *C. elegans* gonads for spreads, we employed an alternative method for disrupting worms, using a 125V ~ 60Hz drill capable of achieving 1,600 rotations per minute. Briefly, we synchronized worms by using the standard bleaching protocol (24) and allowed worms grow to adulthood (L4 + 24 hours). The worms were then washed with dissection solution into a 1.7 mL Eppendorf tube suspended in an ethanol ice bath. The worms were then disrupted using a 1/64 inch bit on the drill with its maximum power by angling the drill bit against the Eppendorf tube wall. 3 µL aliquots were taken from the tube every 20 seconds and monitored microscopically until most of the gonads had been extruded from the worms during the drill-induced disruption.

FISH experiments

Barcoded Oligopaint probes targeting a 1 Mb segment of chromosome II (genomic coordinates 11,500,001-12,500,001) were generated as in (25). Gonads from animals at 24 hours after L4 were dissected on a coverslip and fixed in 1% paraformaldehyde for 5 min. A slide (Superfrost Plus) was then placed on the coverslip and immersed in liquid N_2. The sample was then incubated in −20°C methanol for 2 minutes and rehydrated by placing in PBST for at least 10 minutes. Next, the sample was incubated in 0.1 M HCl for 5 minutes and washed in PBST 3 times for 5 minutes each. The samples were then incubated for 5 minutes each in 2x SSCT (2x saline sodium citrate with 0.1% Tween) solutions with increasing concentrations of formamide: 0%, 5%, 10%, 25%, and 50%. The sample was then incubated in a prewarmed 42°C solution of 50% formamide in 2x SSCT for 1 hour. 2 µL of Oligopaint probe (1,000 ng/µL in dH2O) was diluted into 30 µL of hybridization solution (50% formamide, 10% Dextran Sulfate, 2x SSC, 0.1% Tween-20) for each slide. After 1 hour incubation, slides were taken out of the 50% formamide solution, wiped, and incubated in 95% ethanol for 5 minutes. Then, the probe hybridization solution was applied to the sample with a coverslip, and the sample was denatured for 10 minutes at 77°C on a heat block. After denaturing, the sample was incubated with the probe hybridization solution at 42°C overnight. The next day, samples were washed 2 times in 42°C 50% formamide in 2x SSCT for 30 minutes each, and the coverslip was removed from the slide. Then, the sample was incubated for 5 minutes each in solutions with decreasing concentrations of formamide in 2x SSCT: 25%, 10%, and 5%. Samples were then washed 2 times for 10 minutes each in 2x SSCT. The Oligopaint probes were visualized by hybridizing Cy3-labelled oligos (agctgatcgtggcgttgatg) to the Oligopaint probe barcode sequence. To do this, the Cy3-labelled probes (diluted 1:1000 in 25% ethylene carbonate in 2x SSC) were applied to the sample with a coverslip and incubated for 15 minutes. Then, the sample was washed and the coverslip was removed by incubating in 30% formamide solution in 2x SSCT for 3 min. The samples were then washed twice in 2x SSC and mounted in Vectashield.

For quantification of pairing between FISH signals, gonads were divided into 6 zones. Zone 1 corresponds to the distal tip region of the gonad with only premeiotic nuclei. The gonad region extending from the transition zone to the end of the pachytene stage was split up into 5 equally sized regions, Zones 2-6. The stitched image of the gonad was cropped into zones, peaks of FISH signals were identified using ImageJ plugin 3D Maxima Finder (26). Each identified peak was manually assigned to a nucleus, and distances between homologous signal peaks in the same nucleus were calculated.

Image Acquisition

For spread nuclei, imaging, deconvolution, stitching and 3D-SIM reconstruction were performed as in (23). Spreading results in squashing of *C. elegans* germline nuclei from 5 to 1-2 µm in thickness. 3D-SIM images were obtained as 125 nm spaced Z-stacks, using a 100x NA 1.40 objective on a DeltaVison OMX Blaze microscopy system, 3D-reconstructed and corrected for registration using SoftWoRx. For display, images were projected using maximum intensity projection in ImageJ or SoftWoRx.

For imaging of whole-mount gonads. wide field (WF) images were obtained as 200 nm spaced Z-stacks, using a 100x NA 1.40 objective on a DeltaVison OMX Blaze microscopy system, deconvolved and corrected for registration using SoftWoRx. Subsequently, gonads were assembled using the “Grid/Collection” plugin (27) in ImageJ. For display, assembled gonads were projected using maximum intensity projection in ImageJ.

For display, contrast and brightness were adjusted in individual color channels using ImageJ.

Quantification of RAD-51 Foci and COSA-1 Foci

For quantification of RAD-51 foci in whole-mount gonads, at least three gonads were counted per genotype. Gonads were divided into seven zones: the premeiotic zone (PM), which includes all nuclei prior to the transition zone (where nuclei enter meiotic prophase), and six consecutive equal-sized zones encompassing the region of the gonad from the transition zone to the end of the pachytene

stage. For the GFP::COSA-1 experiments, foci were counted in nuclei within the last six cell rows of the gonad.

Identification of DSB Protein Foci and Object-Based Colocalization Analysis

For Figures 5 and 6, images were analyzed using an object-based colocalization analysis pipeline that combined standard functions available in ImageJ in conjunction with a custom Python script. A detailed description of the colocalization analysis pipeline is presented in Supplemental Figure 3. For these analyses, 32-bit Z-stacks of SIM images of immunofluorescence signals for at least two different antibodies detecting DSB proteins (C1 and C2). were imported into ImageJ (28, 29) with the Fiji distribution (30). The signal maxima for each channel, identified as foci by the image analysis pipeline were qualitatively compared to the original image to verify accurate identification of foci.

For colocalization analysis of DSB-2 and DSB-3::GFP foci on super-spread nuclei (Supplemental Figure S5), the same pipeline was used, except that foci were analyzed within 3.43 x 3.43 μm square ROIs located entirely within the spread (1-3 ROIs per nucleus).

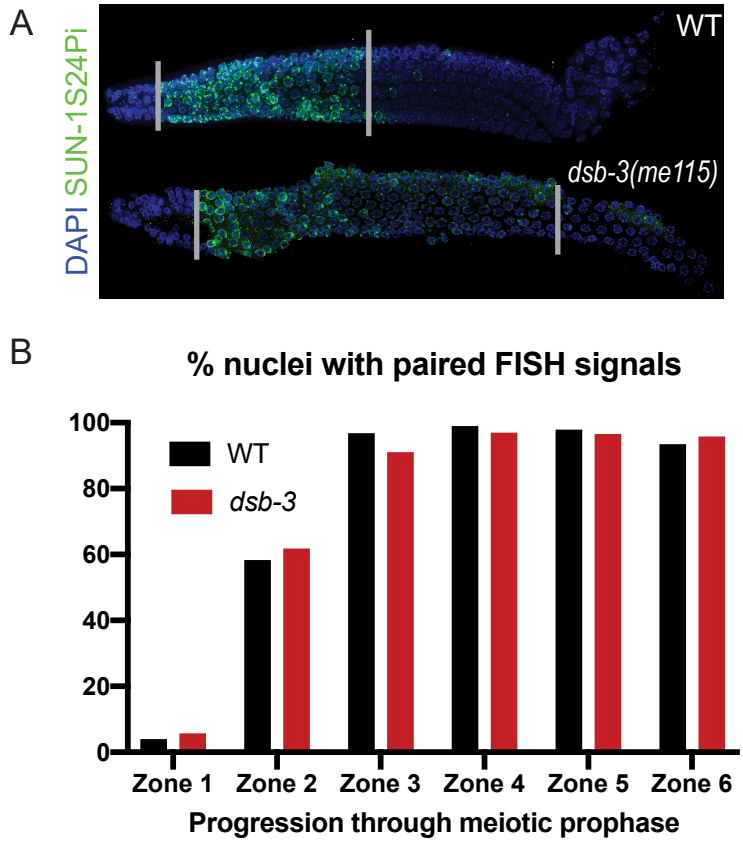

Fig. S1. Meiotic prophase progression and homolog pairing in the *dsb-3(null)* mutant. (A) Immunofluorescence images of whole-mount hermaphrodite gonads (from distal tip to end of pachytene) stained with DAPI and antibodies detecting SUN-1 Ser24 Pi, an indicator of CHK-2 activity detected from the onset of meiotic prophase through the early pachytene stage (21, 31). *dsb-3(me115)* mutant germlines shown an extension of this marker relative to WT, reflecting operation of a crossover assurance checkpoint/surveillance mechanism that prolongs the early pachytene stage in response to one or more chromosome pairs lacking crossover-competent recombination intermediates (15, 16, 31). (B) Quantification of homolog pairing assayed by FISH. Gonads were divided into 6 zones: Zone 1 corresponds to the distal tip region of the gonad with only premeiotic nuclei, and the gonad region extending from the transition zone to the end of the pachytene stage was split up into 5 equally sized regions, Zones 2-6. The stitched image of the gonad was cropped into zones, and peaks of FISH signals were identified using ImageJ plugin 3D Maxima Finder. Each identified peak was manually assigned to a nucleus, and distances between homologous signal peaks in the same nucleus were calculated. FISH signals from homologous chromosomes were considered paired if they were separated by ≤ 0.7 μm. Numbers of nuclei scored for WT: zone 1, n=180; zone 2, n=201; zone 3, n=180; zone 4, n=178; zone 5, n=180; zone 6, n=167. Numbers of nuclei scored for *dsb-3*: zone 1, n=159; zone 2, n=180; zone 3, n=155; zone 4, n=160; zone 5, n=143; zone 6, n=117.

A

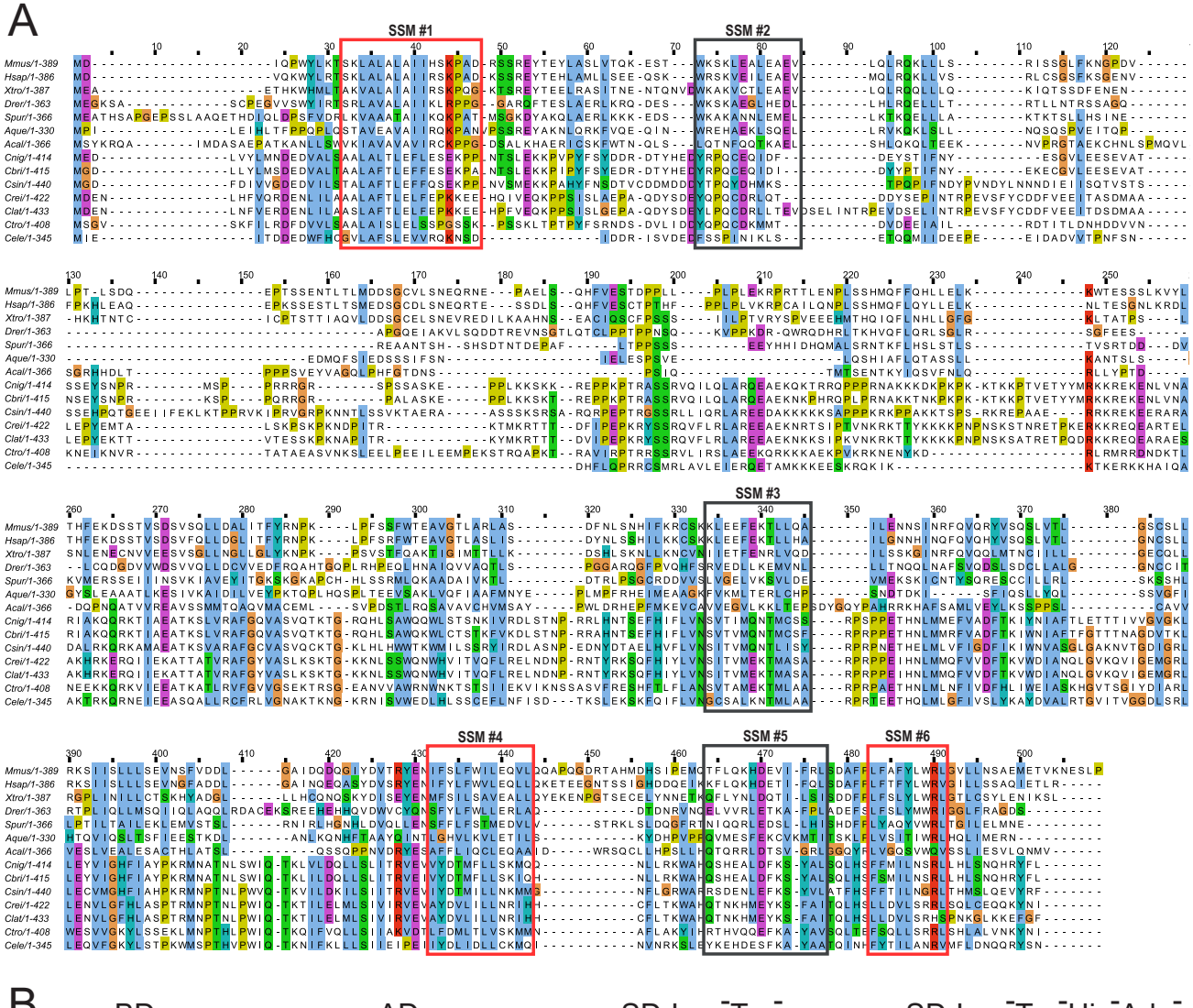

B

BD	AD
SPO-11 (Δ1-47)	AD
DSB-1	AD
DSB-2	AD
DSB-3	AD
BD	SPO-11 (Δ1-47)
BD	DSB-1
BD	DSB-2
BD	DSB-3

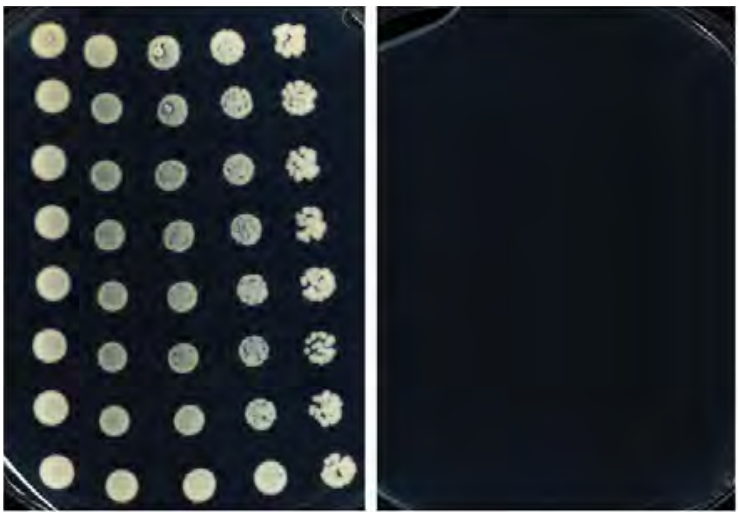

Fig. S2. Alignment of MEI4 and DSB-3 orthologs, and Y2H controls. (A) Multiple sequence alignment generated with MAFFT Version 7.0 with the ClustalX coloring scheme. Protein sequences included in the multiple sequence alignment were from the following species: Vertebrates: *Mus musculus, Homo sapiens, Xenopus tropicalis, Danio rerio*; marine invertebrates: *Strongylocentrotus purpuratus, Amphimedon queenslandica, Aplysia californica*; Nematodes of the genus *Caenorhabditis*: *C. nigoni, C. briggsae, C. sinica, C. remanei, C. latens, C. tropicalis, C. elegans*. The outlined boxes indicate the positions of the SSMs that were previously defined for MEI4 orthologs from diverse species. Red boxes indicate cases where the SSM includes at least 5 amino acid residues that are conserved or exhibit similar electrophysiological properties in at least 85% of the aligned sequences. Gray boxes indicate cases where these thresholds are not met. (B) Negative controls for yeast two-hybrid assays, showing lack of auto-activation for cells containing the indicated constructs.

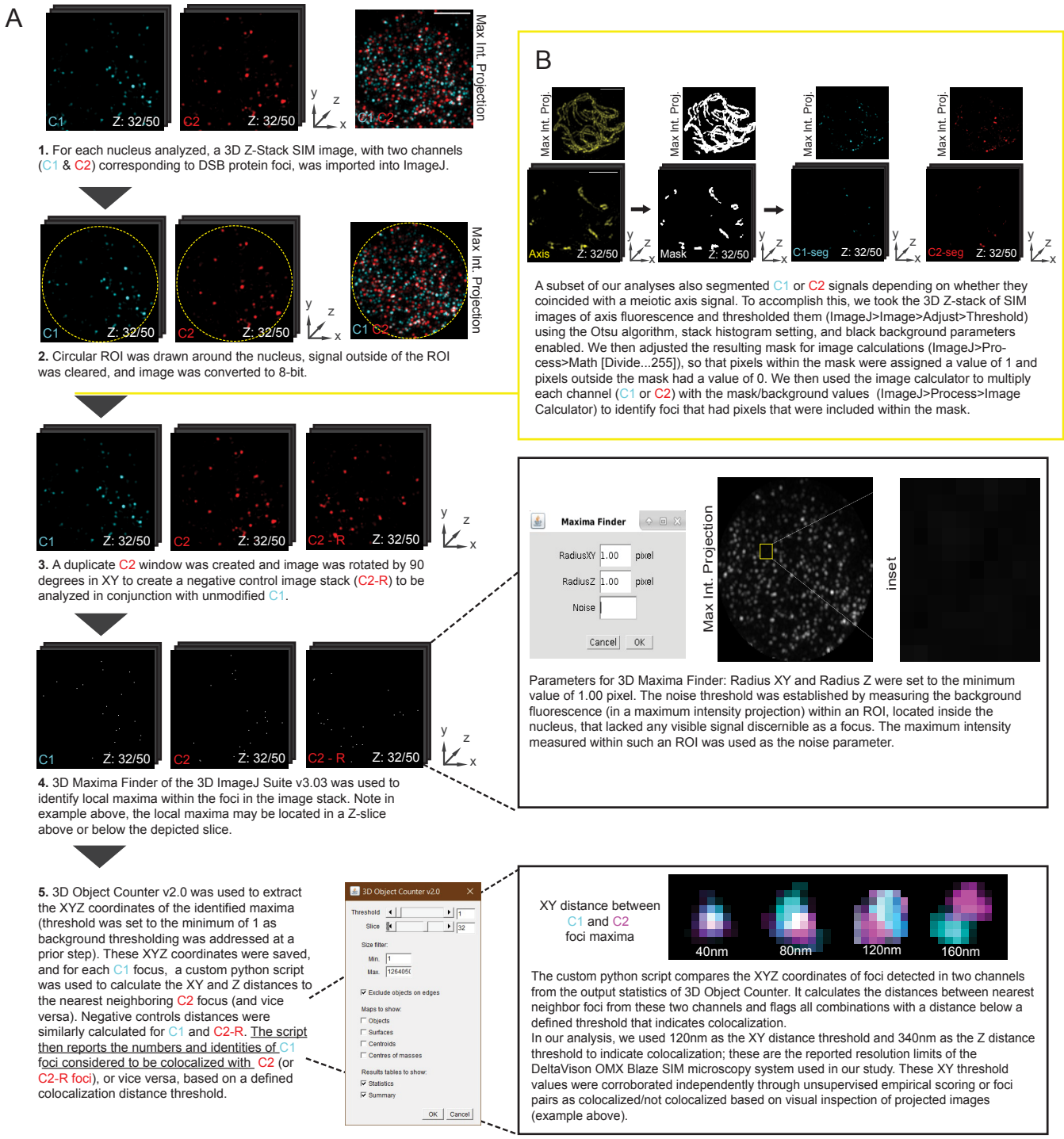

Fig. S3. 3D Object-Based Colocalization Analysis Pipeline for SIM images of DSB protein foci in spread nuclei. (A) A schematic showing the general pipeline used for colocalization analyses. ImageJ plugins used were 3D Maxima Finder (26) and the 3D Object Counter (32). (B) Yellow box indicating protocol used in a subset of our analyses in which images were additionally segmented to identify DSB protein foci that coincided with the axis signal; the Otsu method (33) was used in our thresholding process for this segmentation.

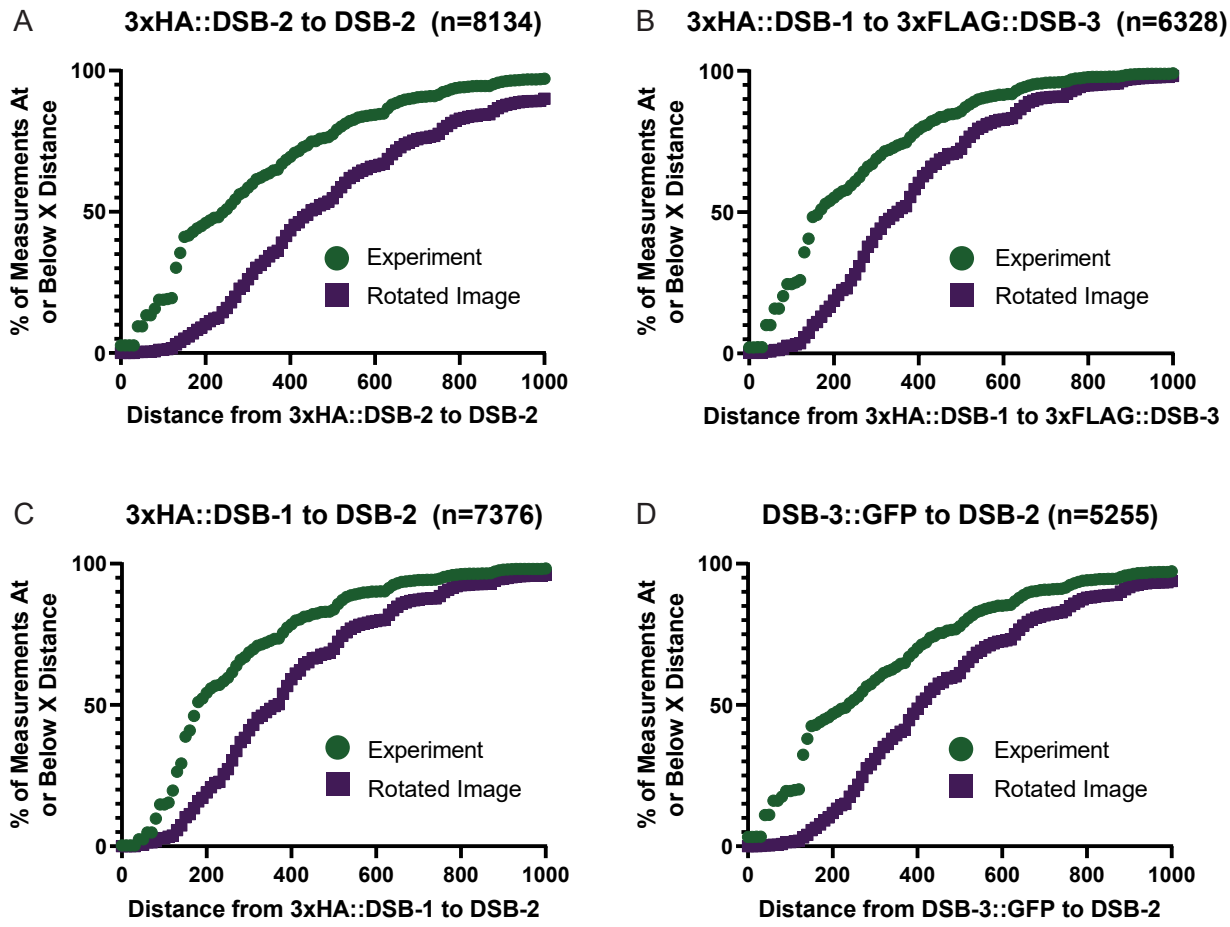

Fig. S4. Cumulative distribution plots for the distances from each Channel 1 DSB protein focus to its nearest neighbor Channel 2 focus. The x-axis represents the distances between nearest neighbor foci pairs, and the y-axis indicates the percentage of measurements at or below the given distance on the x-axis. Experimental data are depicted in green circles and values for the corresponding negative control rotated images are indicated with purple squares. (A) The cumulative distribution of distances between 3xHA::DSB-2 mAB foci and nearest neighbor DSB-2 pAB foci. (B) The cumulative distribution of distances between 3xHA::DSB-1 foci and nearest neighbor 3xFLAG::DSB-3 foci. (C) The cumulative distribution of distances between 3xHA::DSB-1 foci and nearest neighbor DSB-2 pAB foci. (D) The cumulative distribution of distances between DSB-3::GFP foci and nearest neighbor DSB-2 pAB foci.

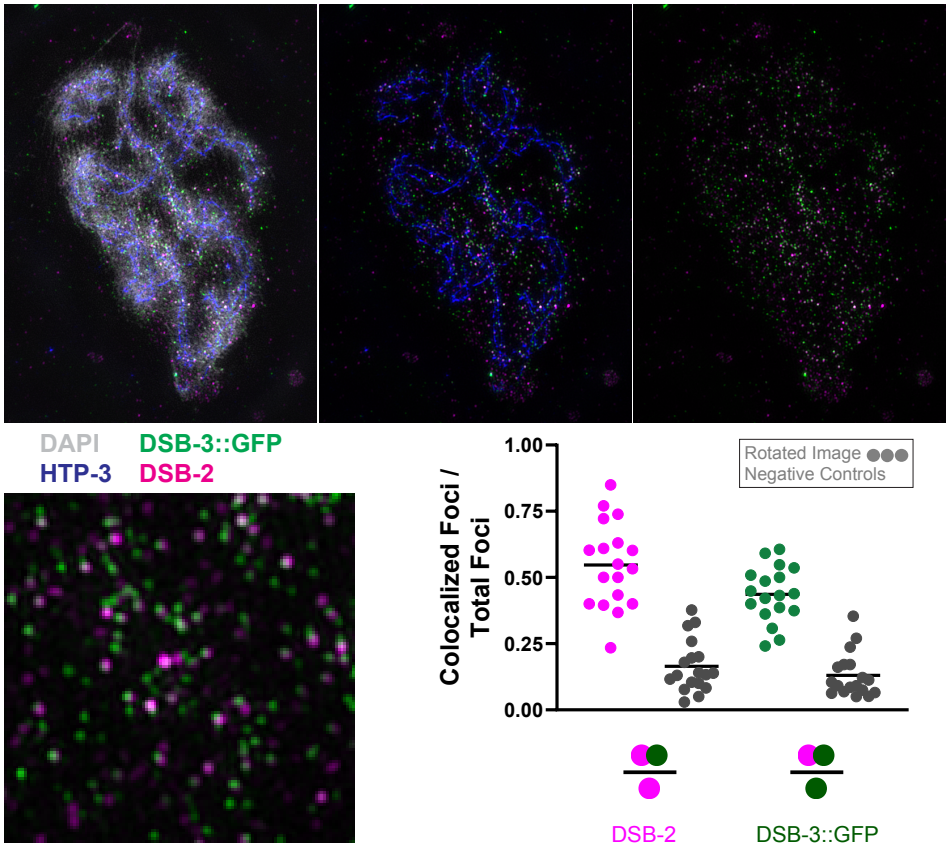

Fig. S5. Colocalization analysis for DSB-2 and DSB-3::GFP on super-spread nuclei. Images depict a super-spread nucleus (top) and an inset from the same nucleus (bottom), showing DAPI-stained DNA and immunofluorescence signals corresponding to DSB-2, DSB-3::GFP, and axis protein HTP-3. The graph shows the fraction of DSB-2 foci (magenta) within a given ROI that are colocalized with a DSB-3::GFP focus (green), and vice versa, together with their paired negative controls (represented by grey data points).

Table S1. Summary of information relevant to the CRISPR/Cas9 edits created for this work. Information includes: a) sequence of the cRNA used in the injection mixture; b) sequence of the edit created and description of its effect on the gene and encoded protein; c) sequences of primers used for mutation detection and verification of edits via Sanger sequencing.

***dsb-1(me124) [3xha::dsb-1]* IV**

crRNA	CACUGGAGUGUCUGCAAUUC
Edit	ATGtatccatacgatgtcccagattacgcttacccatatgacgttccagactatgcctatccatacgatgtcccagattacgctTTTCCTGA**G**TT**A**CA**A**AC**G**CT**T**CA**A**TG
Description	Insertion of 3 N-terminal HA tags underlined and silent mutations introduced to the guide in bold.
Primers	TGTGAATCATTGCTCCCAAG, CCGTCAGCTTCCTGCTATTC

***dsb-3(me125) [3xflag::dsb-3]* IV**

crRNA	GAUCGAAAUUACCGAUGAUG
Edit	ATGgattataaagacgatgacgataagcgtgactacaaggacgacgacgacaagcgtgattacaaggatgacgatgacaagATCGAAATTACCGATGATGA**A**G
Description	Insertion of 3 N-terminal FLAG tags underlined and a silent PAM mutation in bold.
Primers	TTTTCCCGAAACACGATTCT, TTCGGAGTTACGACATCTGC

***dsb-3(me115)* IV**

crRNA	GAUCGAAAUUACCGAUGAUG
Edit	ATGATCGAAATTACCGATGATGAGGACTG**A**TTCC*GGTCTC*TGACTGACTGAACTGC~~T~~GTGTCTTAGCGTTTT
Description	*Leu9X* in bold: Insertion of a BsaI restriction site in italics; STOP codons in +1, +2, +3 frame underlined; and a silent PAM mutation in strikethrough.
Primers	ACACACGCCATCAAGAAAAGCA, TGTGAAGGAAACCGAGTTCCC

***dsb-2(me132) [3xha::dsb-2]* IV**

crRNA	UGUAGUACAUCUCAACUUUC
Edit	ATGtatccatacgatgtcccagattacgcttacccatatgacgttccagactatgcctatccatacgatgtcccagattacgctAGTGCACGTGG**A**CT
Description	Insertion of 3 N-terminal HA tags underlined and silent PAM mutation in bold.
Primers	TGAAGGGACCTGCGCGATGTTT, ATTGCGGTGTCCAGCAGGCATC

SI References

1. S. Brenner, The genetics of Caenorhabditis elegans. *Genetics* **77**, 71–94 (1974).

2. C. Frøkjaer-Jensen, *et al.*, Single-copy insertion of transgenes in Caenorhabditis elegans. *Nat. Genet.* **40**, 1375–1383 (2008).

3. C. Frøkjær-Jensen, *et al.*, An Abundant Class of Non-coding DNA Can Prevent Stochastic Gene Silencing in the C. elegans Germline. *Cell* **166**, 343–357 (2016).

4. C. Engler, R. Kandzia, S. Marillonnet, A One Pot, One Step, Precision Cloning Method with High Throughput Capability. *PLoS ONE* **3**, e3647 (2008).

5. A. Paix, A. Folkmann, D. Rasoloson, G. Seydoux, High Efficiency, Homology-Directed Genome Editing in *Caenorhabditis elegans* Using CRISPR-Cas9 Ribonucleoprotein Complexes. *Genetics* **201**, 47–54 (2015).

6. J. A. Arribere, *et al.*, Efficient Marker-Free Recovery of Custom Genetic Modifications with CRISPR/Cas9 in *Caenorhabditis elegans*. *Genetics* **198**, 837–846 (2014).

7. A. M. Villeneuve, A cis-acting locus that promotes crossing over between X chromosomes in Caenorhabditis elegans. *Genetics* **136**, 887–902 (1994).

8. G. A. Auwera, *et al.*, From FastQ Data to High-Confidence Variant Calls: The Genome Analysis Toolkit Best Practices Pipeline. *Curr. Protoc. Bioinforma.* **43** (2013).

9. M. A. DePristo, *et al.*, A framework for variation discovery and genotyping using next-generation DNA sequencing data. *Nat. Genet.* **43**, 491–498 (2011).

10. A. McKenna, *et al.*, The Genome Analysis Toolkit: A MapReduce framework for analyzing next-generation DNA sequencing data. *Genome Res.* **20**, 1297–1303 (2010).

11. B. Langmead, S. L. Salzberg, Fast gapped-read alignment with Bowtie 2. *Nat. Methods* **9**, 357–359 (2012).

12. P. Cingolani, *et al.*, A program for annotating and predicting the effects of single nucleotide polymorphisms, SnpEff: SNPs in the genome of Drosophila melanogaster strain w1118; iso-2; iso-3. *Fly (Austin)* **6**, 80–92 (2012).

13. J. B. Bessler, K. C. Reddy, M. Hayashi, J. Hodgkin, A. M. Villeneuve, A Role for *Caenorhabditis elegans* Chromatin-Associated Protein HIM-17 in the Proliferation *vs* . Meiotic Entry Decision. *Genetics* **175**, 2029–2037 (2007).

14. F. Gabler, *et al.*, Protein Sequence Analysis Using the MPI Bioinformatics Toolkit. *Curr. Protoc. Bioinforma.* **72**, e108 (2020).

15. S. Rosu, *et al.*, The C. elegans DSB-2 Protein Reveals a Regulatory Network that Controls Competence for Meiotic DSB Formation and Promotes Crossover Assurance. *PLoS Genet.* **9**, e1003674 (2013).

16. E. L. Stamper, *et al.*, Identification of DSB-1, a Protein Required for Initiation of Meiotic Recombination in Caenorhabditis elegans, Illuminates a Crossover Assurance Checkpoint. *PLoS Genet.* **9**, e1003679 (2013).

17. R. Yokoo, *et al.*, COSA-1 Reveals Robust Homeostasis and Separable Licensing and Reinforcement Steps Governing Meiotic Crossovers. *Cell* **149**, 75–87 (2012).

18. C. M. Phillips, *et al.*, HIM-8 Binds to the X Chromosome Pairing Center and Mediates Chromosome-Specific Meiotic Synapsis. *Cell* **123**, 1051–1063 (2005).

19. A. J. MacQueen, *et al.*, Chromosome Sites Play Dual Roles to Establish Homologous Synapsis during Meiosis in C. elegans. *Cell* **123**, 1037–1050 (2005).

20. M. P. Colaiácovo, *et al.*, Synaptonemal Complex Assembly in C. elegans Is Dispensable for Loading Strand-Exchange Proteins but Critical for Proper Completion of Recombination. *Dev. Cell* **5**, 463–474 (2003).

21. A. M. Penkner, *et al.*, Meiotic Chromosome Homology Search Involves Modifications of the Nuclear Envelope Protein Matefin/SUN-1. *Cell* **139**, 920–933 (2009).

22. E. Martinez-Perez, HTP-1-dependent constraints coordinate homolog pairing and synapsis and promote chiasma formation during C. elegans meiosis. *Genes Dev.* **19**, 2727–2743 (2005).

23. D. Pattabiraman, B. Roelens, A. Woglar, A. M. Villeneuve, Meiotic recombination modulates the structure and dynamics of the synaptonemal complex during C. elegans meiosis. *PLOS Genet.* **13**, e1006670 (2017).

24. T. Stiernagle, Maintenance of C. elegans. *WormBook* (2006) https:/doi.org/10.1895/wormbook.1.101.1 (December 20, 2020).

25. A. Woglar, *et al.*, Quantitative cytogenetics reveals molecular stoichiometry and longitudinal organization of meiotic chromosome axes and loops. *PLOS Biol.* **18**, e3000817 (2020).

26. J. Ollion, J. Cochennec, F. Loll, C. Escudé, T. Boudier, TANGO: a generic tool for high-throughput 3D image analysis for studying nuclear organization. *Bioinformatics* **29**, 1840–1841 (2013).

27. S. Preibisch, S. Saalfeld, P. Tomancak, Globally optimal stitching of tiled 3D microscopic image acquisitions. *Bioinforma. Oxf. Engl.* **25**, 1463–1465 (2009).

28. C. T. Rueden, *et al.*, ImageJ2: ImageJ for the next generation of scientific image data. *BMC Bioinformatics* **18**, 529 (2017).

29. C. A. Schneider, W. S. Rasband, K. W. Eliceiri, NIH Image to ImageJ: 25 years of image analysis. *Nat. Methods* **9**, 671–675 (2012).

30. J. Schindelin, *et al.*, Fiji: an open-source platform for biological-image analysis. *Nat. Methods* **9**, 676–682 (2012).

31. A. Woglar, *et al.*, Matefin/SUN-1 Phosphorylation Is Part of a Surveillance Mechanism to Coordinate Chromosome Synapsis and Recombination with Meiotic Progression and Chromosome Movement. *PLoS Genet.* **9**, e1003335 (2013).

32. S. Bolte, F. P. Cordelières, A guided tour into subcellular colocalization analysis in light microscopy. *J. Microsc.* **224**, 213–232 (2006).

33. N. Otsu, A Threshold Selection Method from Gray-Level Histograms. *IEEE Trans. Syst. Man Cybern.* **9**, 62–66 (1979).